Science of the Total Environment 802 (2022) 149726

Contents lists available at ScienceDirect

Science of the Total Environment

journal homepage: www.elsevier.com/locate/scitotenv

Predicting rice yield at pixel scale through synthetic use of crop and deep learning models with satellite data in South and North Korea

Seungtaek Jeong [a], Jonghan Ko [b,1], Jong-Min Yeom [a,*]

[a] Satellite Application Division, Korea Aerospace Research Institute, 169-84 Gwahak-ro, Yuseong-gu, Daejeon 34133, Republic of Korea
[b] Applied Plant Science, Chonnam National University, 77 Yongbong-ro, Buk-gu, Gwangju 61186, Republic of Korea

HIGHLIGHTS

- Pixel-scale rice yield was predicted by combining deep learning and crop models.
- Scalable rice yields from a crop model were used as target labels for deep learning.
- A hybrid structure of LSTM and 1D-CNN was effective for early rice yield prediction.
- The model showed reliable early prediction accuracy (R^2 = 0.86, RMSE = 0.61 Mg ha^{-1}).
- Relative importance of inputs help describe notable differences in yield conditions.

GRAPHICAL ABSTRACT

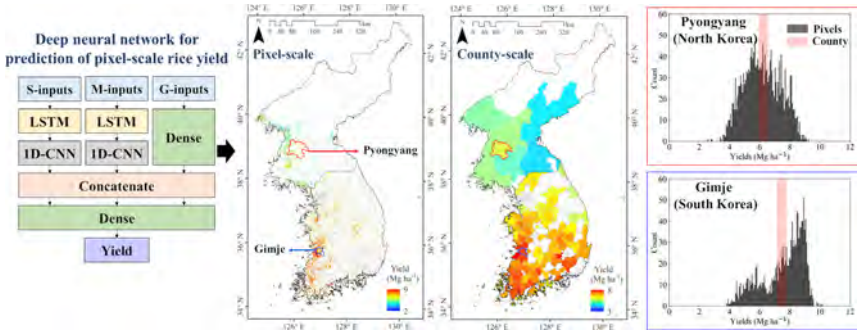

ARTICLE INFO

Article history:
Received 15 April 2021
Received in revised form 11 August 2021
Accepted 13 August 2021
Available online 19 August 2021

Editor: Jurgen Mahlknecht

Keywords:
Crop yield prediction
Data driven model
Crop model
Remote sensing
Korean peninsula

ABSTRACT

Prediction of rice yields at pixel scale rather than county scale can benefit crop management and scientific understanding because it is useful for monitoring how crop yields respond to various agricultural systems and environmental factors. In this study, we propose a methodology for the early prediction of rice yield at pixel scale combining a crop model and a deep learning model for different agricultural systems throughout South and North Korea. Initially, satellite-integrated crop models were applied to obtain a pixel-scale reference rice yield. Then, the pixel-scale reference rice yields were used as target labels in the deep learning model to leverage the advantages of crop models. Models of five different deep learning network architectures were employed to help determine the hybrid structure of long-short term memory (LSTM) and one-dimensional convolutional neural network (1D-CNN) layers by predicting the optimal model about two months ahead of harvest time. The suggested model showed good performance [R^2 = 0.859, Nash-Sutcliffe model efficiency = 0.858, root mean squared error = 0.605 Mg ha^{-1}], with specific spatial patterns of rice yields for South and North Korea. Analysis of the relative importance of the input variables showed the water-related index and maximum temperature in North Korea and the vegetation indices and geographic variables in South Korea to be crucial for predicting rice yields. The proposed approach successfully predicted and diagnosed rice yield at the pixel scale for inaccessible locations where reliable ground measurements are not available, especially North Korea.

* Corresponding author.
E-mail address: yeomjm@kari.re.kr (J.-M. Yeom).
[1] Equal correspondence goes to this author.

https://doi.org/10.1016/j.scitotenv.2021.149726

1. Introduction

Reliable prediction of crop yields can help farmers diagnose crop conditions and adopt necessary measures for better production as well as enable policymakers to effectively manage local food supplies, ensure timely import and exports, and achieve food security (Lobell and Asner, 2003). Moreover, the recent emergence of critical issues such as climate change, severe droughts, rising temperatures, and increased frequency of extreme weather events has posed significant challenges to the reliable prediction of crop yield (Lobell et al., 2014; Jiang et al., 2020). Therefore, considerable effort is presently being devoted to crop yield prediction. In particular, the use of satellite images, which is the only means for predicting crop yields in large and inaccessible areas, has gained attraction (Ferencz et al., 2004; Bolton and Friedl, 2013; Guan et al., 2017). However, accurate prediction remains challenging owing to the necessity of considering numerous environmental factors, cropping systems, management practices, model uncertainties, and unpredictable climate change issues (Lichtenthaler, 1996; Kogan et al., 2012). Hence, an effective approach for crop yield prediction is required (Filippi et al., 2019).

Current methods for predicting spatial crop yield using satellite images are classified into two types (Jeong et al., 2016; Gao et al., 2020): process-based crop modeling and empirical regression. Process-based crop models can simulate continuous crop development, growth, and yield using algorithms and specific parameters associated with crop growth by linking leaf area index (LAI) and vegetation indices (VIs) from satellite data (Doraiswamy et al., 2004, 2005). Although crop models have shown reliable results at a single point scale (Zhao et al., 2013; Huang et al., 2014), they are limited by difficulties in obtaining various spatial inputs and complicated crop parameters, such as soil moisture and physical properties, fertilizer condition, or plant density (Bose et al., 2016; Cao et al., 2021). Furthermore, most process-based crop models require data on entire periods of phenological environment variables for simulation. In terms of prediction within a given season, acquiring the input variables from the prediction time to the harvest time is the main problem. Crop yield can be forecasted through assimilating remotely sensed data into crop growth model at the regional scale (Huang et al., 2019). In contrast, empirical regression methods employ relatively simple input dimensions based on single or multiple regression approaches. They usually predict crop yield from the empirical relationship of VIs and environmental factors with actual measurements of crop yield and are relatively easy to apply to various crops, as intricate crop parameters are not essential (Peng et al., 2014; Lobell et al., 2015; Franch et al., 2015). Therefore, such methods are more straightforward for early yield prediction based on a specific crop growth stage (e.g., heading or maturity) compared to process-based crop models that require information on variables covering the entire period. However, as the early prediction of crop yield has a highly complex nonlinear relationship with the input variables, problems arise in terms of resolving various environmental factors and extending the applicability of empirical regression methods (Sun et al., 2019), which are likely to oversimplify that relationship.

Machine learning (ML) algorithms parse and learn data and then use the learning to make decisions based on input variables (Sammut and Webb, 2011). ML can effectively overcome the drawbacks of traditional empirical methods for the prediction of crop yield with satellite images in large areas (Kim et al., 2019; Khaki and Wang, 2019). Artificial neural networks (ANNs), support vector machines (SVMs), and random forest (RF) have long been used in the field of crop yield prediction (Jiang et al., 2004; Vincenzi et al., 2011; Su et al., 2017). These ML techniques can predict crop yields more accurately than existing empirical regression models by addressing the non-linear relationship between the input environment variables and the yield without the complicated crop growth parameters used in the process-based crop models (Kumar et al., 2019). However, problems such as overfitting, prolonged training, and relatively few hidden layers limit their ability to solve non-linear problems and perform crop yield prediction in large areas (Khaki and Wang, 2019; Nevavuori et al., 2019). Recent breakthroughs in deep learning (DL) techniques based on end-to-end training through deep hidden layers have facilitated sophisticated and accurate crop yield prediction (Cai et al., 2019; Yang et al., 2019; Khaki et al., 2020). Thus, DL is being actively used for crop yield prediction. In particular, comparative studies have verified that DL models have exhibited better performance than existing regression or ML methods in predicting crop yield (Kim et al., 2020; Wolanin et al., 2020; Maimaitijiang et al., 2020).

However, most studies on crop yield prediction based on DL or conventional ML models with satellite images have been conducted at the county scale; input images from satellites were averaged or used as a histogram in administrative districts (Jiang et al., 2020; Cai et al., 2019; Kim et al., 2020). According to Lobell et al. (2015), the primary reasons for preferring the county scale in remote sensing studies were given as follows. (1) the main goal of funders is to characterize production at the aggregate scale, e.g., the county scale, and (2) estimation of ground-based crop yield for field scales in large areas is extremely difficult compared to that for aggregate political units. From a technical (rather than a policy-based) perspective, it is challenging to obtain the spatiotemporal reference data of crop yield in pixels over a large area, e.g., on a national or continental scale. Therefore, pixel-scale mapping of crop yield has not been widely adopted in deterministic or data-driven models, including DL approaches in remote sensing studies. Crop yield prediction at the county scale lacks the significant advantage of satellite images, which allow more efficient pixel-scale indicators to be obtained for precise analysis and diagnosis of crop status. In other words, county-scale prediction is less sensitive to the reduction in rice growth and yield owing to not only climate change effects but also other factors (e.g., pests, diseases, and weeds) because the average values are obtained only within the county. In contrast, estimates based on individual fields or pixels within an agricultural landscape are beneficial for understanding how the crop yield responds to various management and environmental factors (Lobell et al., 2015).

In this study, we propose a novel approach for the early prediction of rice yield at pixel scale through the synthetic use of a crop model and DL model, incorporating satellite images for different agricultural systems in South and North Korea. The specific objectives of this study are as follows: (1) to obtain reliable pixel-scale rice yield as a reference label for DL by leveraging the advantages of the crop model, (2) to determine an optimal DL model by testing five DL structures with different characteristics using the reference data, (3) to perform early prediction of the pixel-scale rice yield and evaluate the model performance, and (4) to analyze the spatial distribution of the rice yield and the relative importance (RI) of the input variables for different agricultural environments in South and North Korea (Yeom et al., 2018; Zhang et al., 2017; Ryu et al., 2019). In particular, we evaluate whether the proposed approach can effectively predict and diagnose rice yields and conditions in the inaccessible areas of North Korea.

2. Materials and methods

2.1. Study area and materials

2.1.1. Study area

In this study, we targeted paddy rice (*Oryza sativa*), which is a major staple grain crop worldwide and in South and North Korea (Xin et al., 2020). The average temperature and precipitation in the study area ranges from 6 to 15 °C and 590 to 1900 mm, respectively. According to the KOrean Statistical Information Service (KOSIS, https://kosis.kr), paddy fields accounted for ~1,436,000–1,531,000 ha of the entire study area, with 865,000–960,000 ha in South Korea and ~ 517,000 ha in North Korea, from 2011 to 2017. The total rice production was ~6,009,000 Mt., ranging from 3,972,000 to 4,006,000 Mt. in South

Korea and from 2,037,000 to 2,192,000 Mt. in North Korea, from 2011 to 2017. The two countries belong to similar climate zones (Peel et al., 2007), dominated by a single rice cropping system owing to the wide temperature ranges and the temporal concentration of precipitation in the summer under the monsoon climate. However, South Korea's rice production is around twice as high as that of North Korea, which has a different agricultural environmental system as per the KOSIS. Paddy fields are widely distributed in the western areas of the Korean peninsula, as most plains are formed mainly in the west (Fig. 1).

2.1.2. Data and pre-processing of input variables

The input variables of each crop model and DL model for estimation of the pixel-scale reference rice yields and its prediction are summarized in Table 1. We resampled the different spatial resolutions of the input variables at a resolution of 500 m for our reference using the nearest-neighbor interpolation method.

2.1.2.1. Vegetation indices and transplanting date variables. The VIs express the crop growth condition on the top of the canopy, reflecting

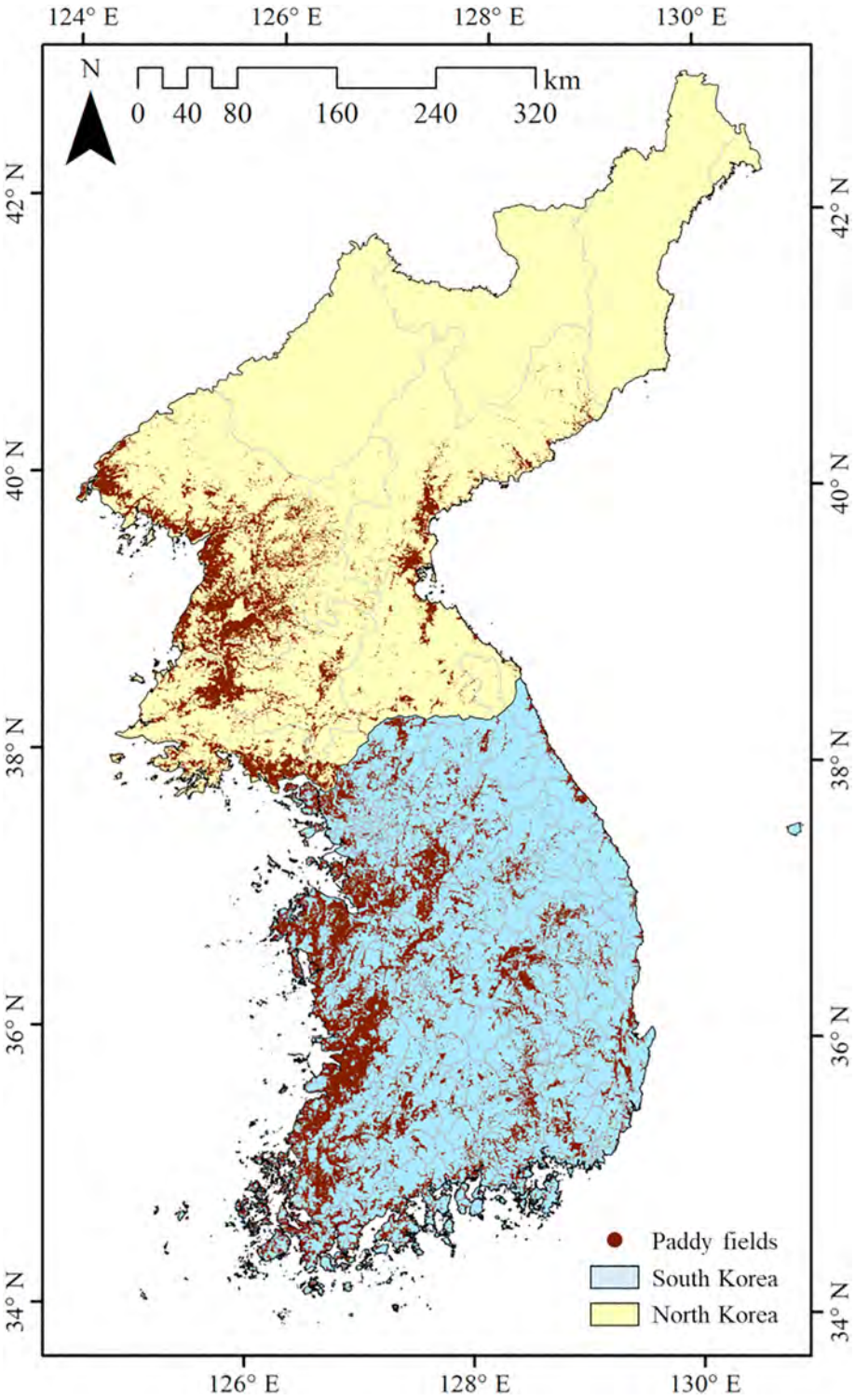

Fig. 1. Spatial distribution of paddy fields based on MODIS satellite images in South and North Korea extracted from the lowland rice extent map of Asia from the International Rice Research Institute.

Table 1
Input variables for both the crop model and the DNN model used for early prediction of pixel-scale rice yield.

Inputs[a]	Resolution (temporal/spatial)	Products
Terra MODIS (MOD09A1)	8-day composite/0.5 km	Vegetation indices, transplanting dates
COMS MI	daily/1 km	Solar radiation
RDAPS	4 times a day/12 km	Minimum and maximum temperatures
IRRI paddy map	One image/0.5 km	Yearly paddy maps
Administrative district map	Vector form	County and province information

[a] MODIS, Moderate resolution imaging spectroradiometer; COMS MI, communication, ocean, and meteorological satellite meteorological imager; RDAPS, regional data assimilation and prediction system; IRRI, international rice research institute.

various environmental or biophysical factors; hence, they are the most crucial determinants for predicting crop yield from remote sensing data. In this study, we used time-series VI data obtained from the Moderate Resolution Imaging Spectroradiometer (MODIS) Version 6 (Terra / MOD09A1) 8-day composite surface reflectance product with a spatial resolution of 0.5 km. The VIs were used as input for estimating LAI in the crop model, and as main data for predicting the rice yield in the DL model. MODIS is the most widely used earth observation system for land surface monitoring; it incorporates the characteristics of seasonal changes in surface vegetation owing to its high temporal resolution (Ren et al., 2008; Jeong et al., 2012; Zhang and Zhang, 2016). The MOD09A1 product consists of seven reflectance wavebands from 469 nm (blue) to 2130 nm (short-wave infrared) with a spatial resolution of 500 m. Based on previous studies using the remote-sensing integrated crop model (RSCM), the five VIs were selected, which have also been commonly used for crop models using satellite images (Jeong et al., 2018); normalized difference vegetation index (NDVI (Rouse, 1974)), optimized soil adjusted vegetation index (OSAVI (Rondeaux et al., 1996)), renormalized difference vegetation index (RDVI (Roujean and Breon, 1995)), modified triangular vegetation index (MTVI1 (Haboudane et al., 2004)), and enhanced vegetation index (EVI (Huete et al., 2002)). These indices are given by the following eqs.

$$\mathrm{NDVI} = \frac{\rho_{NIR} - \rho_{Red}}{\rho_{NIR} + \rho_{Red}}, \tag{1}$$

$$\mathrm{OSAVI} = \frac{\rho_{NIR} - \rho_{Red}}{\rho_{NIR} + \rho_{Red} + 0.16}, \tag{2}$$

$$\mathrm{RDVI} = \frac{\rho_{NIR} - \rho_{Red}}{\sqrt{(\rho_{NIR} + \rho_{Red})}}, \tag{3}$$

$$\mathrm{MTVI1} = 1.2 * [1.2 * (\rho_{NIR} - \rho_{Green}) - 2.5 * (\rho_{Red} - \rho_{Green})], \tag{4}$$

$$\mathrm{EVI} = 2.5 * \frac{\rho_{NIR} - \rho_{Red}}{\rho_{NIR} + 6 * \rho_{Red} - 7.5 * \rho_{Blue} + 1}, \tag{5}$$

where ρ_{Red}, ρ_{NIR}, ρ_{Blue}, and ρ_{Green} are MODIS MOD09A1 reflectance band 1 (620–670 nm), band 2 (841–876 nm), band 3 (495–479 nm), and band 4 (545–565 nm), respectively.

In addition, the land surface water index (LSWI (Gao, 1996)) from the MODIS product was calculated to reflect the crop and soil water status (Chandrasekar et al., 2010) as a water index. It is given by the following equation.

$$\mathrm{LSWI} = \frac{\rho_{NIR} - \rho_{SWIR}}{\rho_{NIR} + \rho_{SWIR}}, \tag{6}$$

where ρ_{SWIR} is MODIS MOD09A1 reflectance band 7 (2105–2155 nm).

LSWI, NDVI, and EVI were additionally used to estimate the rice transplanting date (TPD), which is the main factor indicating when the observed paddy growth began. Xiao et al. (2005) proposed a method for estimating TPD from satellite images, whereby the relationship between LSWI and the VIs (NDVI or EVI) is reversed when irrigation is performed in the paddy fields. In the present work, the TPD was calculated as a date satisfying the following condition. LSWI $+0.05 >$ EVI or NDVI, where 0.05 is a constant for increasing the sensitivity of LSWI in the mixed pixels (Xiao et al., 2005).

2.1.2.2. Meteorological variables. In this study, images from the Meteorological Imager (MI) of the geostationary Communication, Ocean and Meteorological Satellite (COMS) were used to estimate daily solar radiation with a spatial resolution of 1 km. The sun is the main energy resource for photosynthesis in crop canopies and (Yeom et al., 2016) directly influences crop growth and development. This is because solar radiation is the energy source for photosynthesis and environmental controls on vegetation growth and morphogenesis (Yeom et al., 2018). The incident solar radiation was calculated using a physical model by interpreting the radiative effects of atmospheric constituents and clouds from the incoming solar radiation. In the case of clear sky conditions, atmospheric parameterizations were performed by considering the reduction of incoming solar radiation due to atmospheric constituents such as aerosol, water vapor, ozone and Rayleigh scattering. For cloudy atmospheric conditions, cloud attenuation was applied by using a cloud factor consisting of the cloud top reflectance and solar zenith angle. A detailed explanation of the physical model selected for solar radiation has been provided by Yeom et al. (2016).

The minimum (T_{min}) and maximum (T_{max}) temperatures were also employed to estimate the rice growing degree day (GDD), a measure of heat accumulation for estimating the crop development in the crop model, which is also used as an input variable for the DL model. It is given by the following equation.

$$\mathrm{GDD} = (T_{max} - T_{min}) - T_b, \tag{7}$$

where T_b is the crop base temperature (°C) below which plant growth is zero. The data were acquired from the Regional Data Assimilation and Prediction System (RDAPS) developed by the Korea Meteorological Administration (KMA, https://www.kma.go.kr). RDAPS works by receiving initial and boundary weather conditions from the Global Data Assimilation and Prediction System (GDAPS) and provides weather data four times a day at 6 h intervals (00:00, 06:00, 12:00, and 18:00 UTC), based on the four-dimensional variable data assimilation (4D-Var) technique (Elbern et al., 2000) with a spatial resolution of 12 km.

2.1.2.3. IRRI lowland rice extent map. The International Rice Research Institute (IRRI, https://www.irri.org) has provided a lowland rice map with a spatial resolution of 500 m for Asia, which accounts for more than 90% of global rice production (Nelson and Gumma, 2015). This map was developed using the MOD09A1 8-day product, as with the images used in this study, and the Shuttle Radar Topography Mission (SRTM) digital elevation model (DEM). The mapping methodology adopts the approach of using the time series relationship between VIs and LSWI, proposed by Xiao et al. (2005, 2006). The statistical analysis involves overestimation compared to the actual paddy areas, as it is assumed that one 500-m pixel is entirely devoted to paddy; however, the coefficient of determination (R^2) was relatively high, i.e., 0.87 for South Korea and 0.82 for North Korea, in terms of the total area of the provincial paddy fields. Further details regarding the data processing and methodology have been provided by Nelson and Gumma (2015). As only one map composited from 2001 to 2012 was provided, we developed annual paddy maps from 2011 to 2017 using the threshold in the transplanting periods, i.e., maximum EVI > 0.3 (Fig. S1 in the supplementary file), which can exclude non-paddy pixels (Sakamoto et al., 2007) owing to low VIs in the transplanting period caused by irrigated water in the fields (Xiao et al., 2005).

2.1.2.4. Reported statistical rice yield. The reported rice yields were used as ground truth data, which were obtained from the Korean Statistical Information Service (KOSIS) for South Korea and the Food and Agriculture Organization (FAO, http://www.fao.org) and the United States Department of Agriculture (USDA, https://www.usda.gov) for North Korea. The rice yields for South Korea were collected at the county scale, while those for North Korea were collected at the province scale. The total number of counties and provinces in the study areas was 106, including 96 counties in South Korea and 10 provinces in North Korea. The counties where the rice cultivation areas are smaller than 2000 ha in each administrative region were excluded from model training and evaluation because there is a high possibility of errors arising from the mixed pixels for small, fragmented paddies (Jeong et al., 2018). These made up less than about 5% of the entire paddy area considered.

2.2. Methodology

The study process was divided into two steps for the early prediction of rice yield at the pixel scale (Fig. 2). The first step involved producing pixel-scale reference rice yields using theRSCM. The produced yields were used as target labels for the DL model while leveraging the advantages of the crop model. For this purpose, the RSCM calibration and simulation was performed by adjusting the crop growth parameters within an appropriate range based on the reported rice yields. The second step was to find the optimal structures of the DL model for training the reference rice yield and make an early prediction of the rice yields using the DL model at the pixel scale with the same spatial resolution as the input. For reference, we additionally predicted the rice yields at the county scale to highlight the difference between the two distinct approaches. To perform this comparison based on synthetic analysis, all the input variables were averaged by the county units. Finally, we interpreted the environmental variable factors affecting the rice yield in South and North Korea on the basis of the RI for the input variables of the DL model.

2.2.1. Remote-sensing integrated crop model (RSCM)

RSCM, developed by Kim et al. (2015), is a modified version of the GRAMI crop model (Maas, 1992). The RSCM is a process-based model able to simulate continuous crop growth information (e.g., biomass, net primary productivity, evapotranspiration, and yield) using LAI, weather data, and fewer crop-specific parameters compared to other crop models (Kim et al., 2017; Jeong et al., 2020; Yeom et al., 2021). The LAI is a key variable for most crop models because biomass is calculated from the LAI and the final yield is determined from the biomass. A typical feature of the model is the within-season calibration procedure (Maas, 1993), which is formulated to calibrate the simulated LAI in response to remote-sensing observations representing the crop growth, allowing integration with satellite images. RSCM uses the relationship between the ground-measured LAI and several VIs from the satellite based on the log-log linear regression model (Jeong et al., 2018). Using multiple VIs gives a more robust estimate of the LAI, with an ensemble approach based on the four VI-to-LAI relationships (Nguyen et al., 2019). Furthermore, the within-season calibration procedure allows the model to assimilate the remote-sensing information obtained from a variety of platforms, including unmanned aerial vehicles (UAVs) and optical satellites. Further details regarding the RSCM can be found in previous studies (Kim et al., 2015; Kim et al., 2017; Jeong et al., 2020; Yeom et al., 2021).

The model was calibrated and parameterized based on the reported rice yields at the county scale by tuning the crop parameters. Since cropping systems and rice varieties differ for each region, the parameters were adjusted within the allowable range by applying optimal values to each county. The adjusted parameters were applied to pixels for simulating the rice yield using the RSCM. Further details of the crop parameters are provided in Ko et al. (2015) and Jeong et al. (2018).

2.2.2. Deep learning (DL) model

2.2.2.1. Pre-processing of input variables. The input variables are divided into three types according to the time-series intervals (data shapes) of the SIs (S-inputs) at an 8-day temporal resolution, meteorological data (M-inputs) including maximum and minimum temperatures and solar radiation at a daily temporal resolution, and four geospatial information data (G-inputs). The geospatial information data included geographic coordinates (latitude and longitude), county IDs assigned according to administrative districts, and TPDs, which were used to capture the regional characteristics of inherent rice yields depending on the

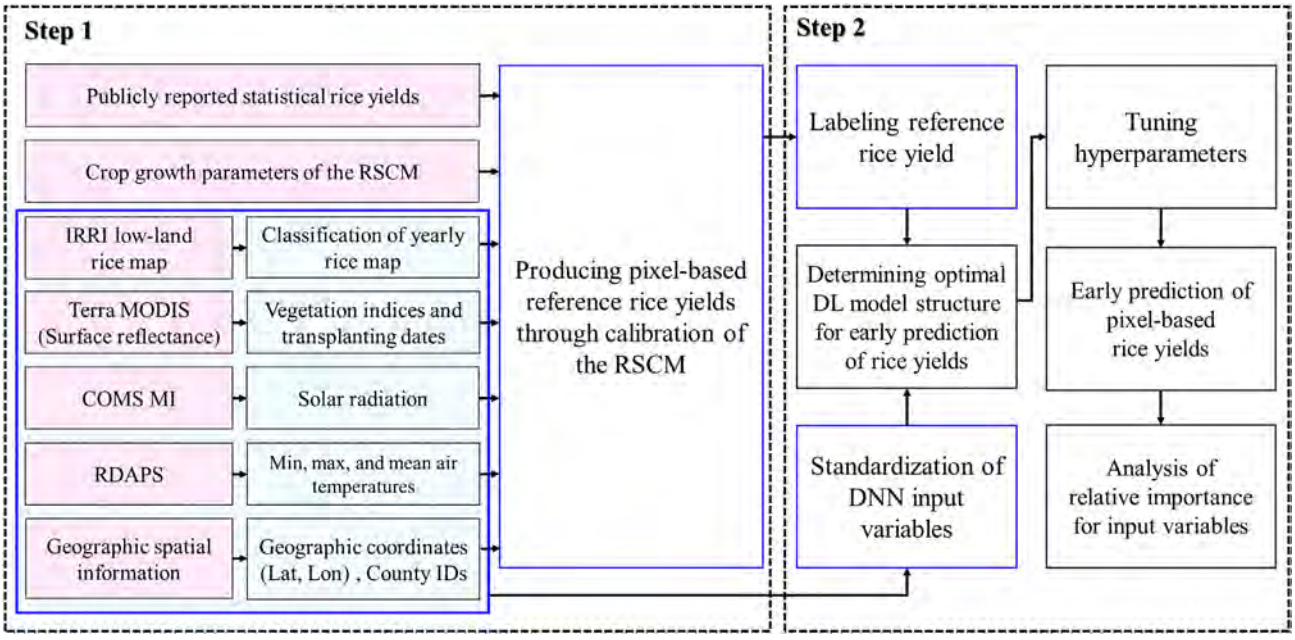

Fig. 2. Workflow for early prediction of the pixel-scale rice yield by combining the RSCM and DL model incorporating satellite images. The blue boxes denote the learning datasets used in the DL model.

agricultural environment system and rice varieties; these would help predict the rice yield by considering the regional characteristics indirectly. Here, it was assumed that similar varieties were cultivated annually in the same region. The entire dataset period ranged from 2011 to 2017 (total of 433,773 pixels) over the classified rice paddy area (Fig. S1 in the supplementary file), using the datasets of 2011 to 2016 for the training (263,232 pixels) and validation (112,815 pixels) of the model. The trained model was applied to the test dataset of 2017 (57,726 pixels) to evaluate its performance. Based on the rice cultivation characteristics of the current study area, the usage period of the time-series variables for early prediction was determined as ranging from May 1 (DOY 121) to the end of August (DOY 240). The overall harvest time of this study area extended from the end of September to the end of October, i.e., the early prediction was obtained around one or two months in advance. The periods of rice cultivation can differ regionally, and we expected the TPDs to consider the feature of temporal variation.

2.2.2.2. DL model structures. When input data of various shapes are used in the DL model, they must be normalized to the same shape. Otherwise, the model should be configured in a structure that can receive multiple input shapes. In this study, the input layers in the common setup of the DL models were configured in multiple forms in accordance with the input shapes, such as the S-input, M-input, and G-input. Then, they were merged into a concatenate layer through each hidden layer. The final rice yields were predicted through additional fully connected (FC) layers after the concatenate layers. The G-input layers were composed of only an FC layer and concatenate layers as they involved only four variables without sequential data. The activation functions employed included the rectified linear unit (ReLU) in the 1D-CNN and FC layers and the hyperbolic tangent (tanh) in the LSTM layers. A batch normalization (BN) layer was added after all the activation layers to avoid the gradient vanishing problem and to accelerate convergence. This methodology is considered to be less affected by the initialization strategy through each output normalization (Ioffe and Szegedy, 2015). The overall structure diagram is shown in Fig. 3.

We tested five different structures to determine the optimal DL structure that could effectively learn the RSCM model and predict yields. Hence, different neural networks were placed between the input and concatenate layers (Fig. 3). The first consisted of only FC layers (Fig. 3A). This is the most basic structure in a multi-layered perceptron and the most frequently used for predicting rice yields (Gao et al., 2020; Khaki and Wang, 2019). The second neural network comprised 1D-CNN layers (Fig. 3B), in which the 1D-CNN was comparable to a recurrent neural network (RNN) in terms of a specific sequence of processing problems, generally requiring less computing power (Wolanin et al., 2020). The third network comprised LSTM layers with feedback connections, in contrast to FFNN (Fig. 3C). LSTM has been reported to show powerful performance in long-term sequential data interpretation (Jiang et al., 2020). In particular, as there are meaningful periods for crops, such as the heading to maturity period, which strongly influence crop yield (Wheeler and Salter, 1974; Fageria, 2007) compared to other crop growth periods, the LSTM considering a long-term sequence has exhibited better performance than the other structures in crop yield prediction (Jiang et al., 2020; Schwalbert et al., 2020). The fourth one was a hybrid model combining the first 1D-CNN and LSTM structures (Fig. 3D). When predicting crop yield using the DL model, a single structure alone is assumed to be limited in terms of improving the model performance; hence, a hybrid approach combining two different structures, such as a CNN and an RNN, has been proposed (Sun et al., 2019; Khaki et al., 2019). This hybrid structure first extracted the spatial features using the CNN and then predicted the crop yield by considering the extracted sequential features using an LSTM. The fifth neural network tested was also a hybrid model combining the first LSTM and 1D-CNN layers (Fig. 3E). We assumed that, in contrast to the first 1D-CNN structure, it would first capture the temporal features from the original inputs and effectively predict the crop yield by extracting the

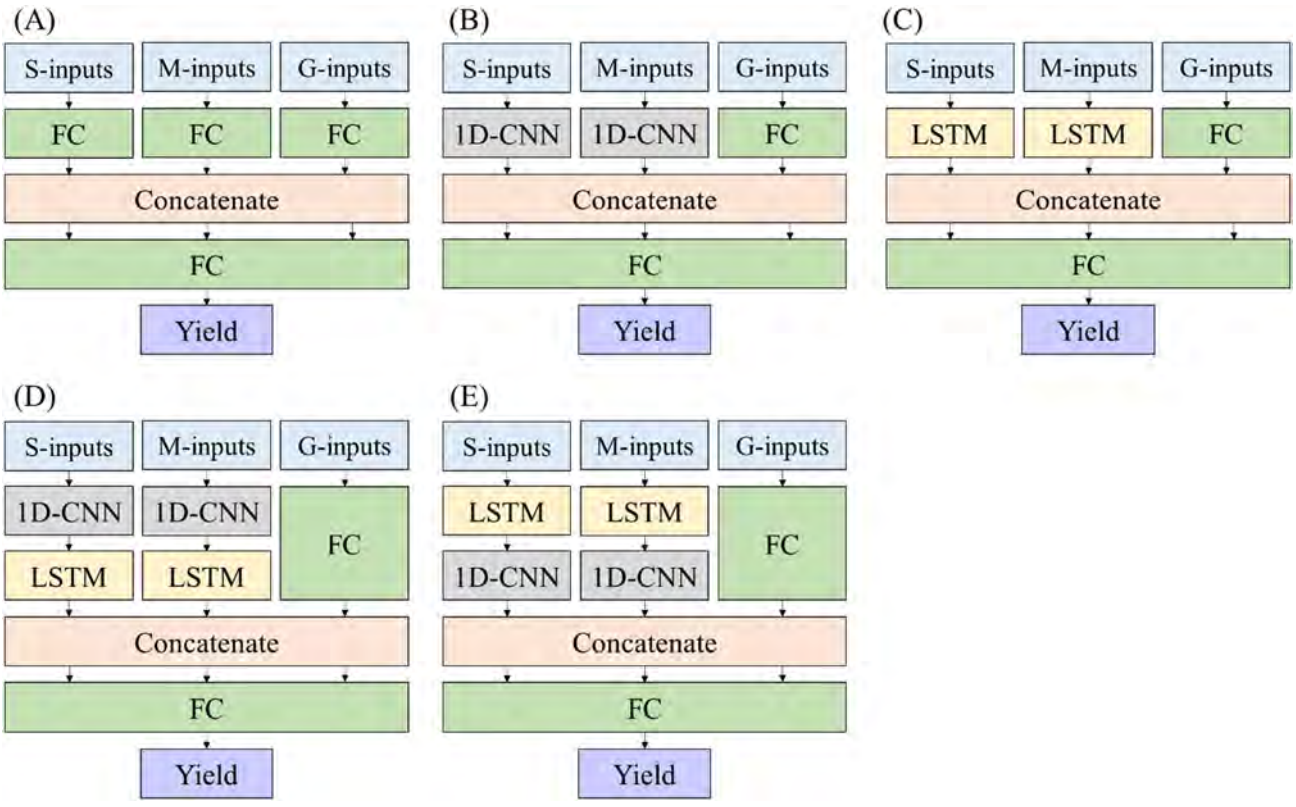

Fig. 3. DL model structures to predict rice yield through combinations of FC, 1D-CNN, and LSTM layers. The S-inputs, M-inputs, and G-inputs are the input dimensions of the spectral (S) indices (VIs and LSWI), meteorological (M) variables (T_{min}, T_{max}, and solar radiation), and geospatial (G) information (geographic coordinates, county IDs, and transplanting date).

meaningful features using a 1D-CNN. For convenience, these five DNN structures were denoted as FFNN, 1D-CNN, LSTM, 1D-CNN + LSTM, and LSTM+1D-CNN.

2.2.2.3. Analysis of the relative importance of input variables in South and North Korea. South Korea is well-equipped with irrigation facilities, and yields are managed well with sufficient fertilizer and pesticides. On the other hand, in North Korea, rice is grown in an environment where water supply is insufficient due to lack of precipitation and poor irrigation facilities in many areas, and yields are not well-managed due to economic problems (Yeom et al., 2018; Ryu et al., 2019). We analyzed the RI of the input variables to determine which factors were considered significant when predicting the rice yield in South and North Korea with different agricultural environments. Compared with conventional empirical and ML models, it is difficult to understand the RI used for prediction and the final perdition in DL models (Jeong et al., 2016). Recently, a method for visualizing the regression activation map of CNN or RNN models has been proposed (Wolanin et al., 2020; Zhang et al., 2018). However, this method was limited to models based on vector datasets and could not be used on 2D images or hybrid models. In the present work, we adopted a commonly used method to obtain the RI of a model, which removes the input variables one by one and estimates the RI of each variable through the degree of error variation (Quintero et al., 2014; Arigbe et al., 2019; Song et al., 2016). The equation employed was as follows.

$$\text{Relative importance (RI)} = \text{MSE}_i \frac{}{\sum_{i=1}^{n}(\text{MSE}_{Reference} - \text{MSE}_i)} * 100\%, \quad (8)$$

where MSE_i, $\text{MSE}_{Reference}$, and n represent the MSE of the dropped input variable, the MSE of all the input variables used in the DL model for the early prediction of the rice yields, and the total number of the input variables, respectively. The RIs were used to interpret the effect of each input variable on the rice yields according to the different agricultural environments for North and South Korea. We also analyzed the indexed error variation maps in which the specific input variables were removed from the model. Here, a large error variation indicates that the dependence on the dropped variable was high; hence, it indirectly indicates the importance of the linked variable, similar to RI.

2.3. Statistical analysis

We evaluated the model performance using the following statistical indices: root-mean-square error (RMSE), coefficient of determination (R^2), and Nash–Sutcliffe model efficiency (NSE). The RMSE is commonly used as an accuracy metric when dealing with the difference between observed and predicted values. R^2 is a measure of the degree to which the simulated data linearly fits the observed data. Its value ranges from 0 to 1; the closer the value is to 1, the stronger is the linear relationship between the observed and simulated values. NSE is a normalized statistic that determines the relative magnitude of the residual variance compared to that of the observed data variance (Nash and Sutcliffe, 1970). This value indicates how well the plot of the observed and simulated data fits the one-to-one line, where the value ranges from – ∞ to 1; the closer the value is to 1, the higher the performance of the model.

3. Results and discussion

3.1. Calibration results for the RSCM

First, we produced pixel-scale reference rice yields based on the abovementioned RSCM calibration before performing early prediction of the rice yields using the DL model. The statistical analysis results for the model calibration were as follows: $R^2 = 0.805$, NSE = 0.770, and RMSE = 0.432 Mg ha^{-1} (Fig. 4). We assumed that the produced pixel-scale rice yields had a reliable statistical agreement with the reported rice yields for both South and North Korea. Thus, the RSCM was well calibrated with the reported yields at the county (or province) scale, enabling us to use the produced rice yields as target labels in the DL model at the pixel scale.

The RSCM was modified and improved from the GRAMI model (Maas, 1992 and 1993) that has proven its reliability in previous studies (Ko et al., 2015; Kim et al., 2017; Jeong et al., 2018; Jeong et al., 2020; Yeom et al., 2021). Although only the yield was targeted in this study, because the proposed approach is a process-based model, various rice growth information can be produced as reference labels. Meanwhile, there is a limitation in that it has been validated only for rice observed through satellite images and the crop growth parameters were defined only for short grain (Japonica) rice varieties that are mainly cultivated in Northeast Asia. However, the crop model can be replaced with other crop models developed at the field scale depending on study aims. Notably, the purpose of using the crop model in our methodology is to deliver training datasets (or reference labels) to the DL model. An important issue in using a crop model is calibrating the parameters carefully and accurately, as the accuracy of the model output directly affects the DL model performance.

3.2. Determination of the DL model for early prediction of rice yield

We compared the early predictions of rice yields simulated using the five DL models (i.e., FFNN, 1D-CNN, LSTM, 1D-CNN + LSTM, and LSTM+1D-CNN). We found that most of the match-up dots of the DL model-simulated rice yields were located around the one-to-one line in comparison with the reference rice yields from the RSCM (Fig. 5). Among the five DL models, LSTM+1D-CNN showed the highest performance, with $R^2 = 0.859$, NSE = 0.858, and RMSE = 0.605 Mg ha^{-1} (Fig. 5E), as the performance of hybrid models able to capture different characteristics was often better than that of a single-structure DL model

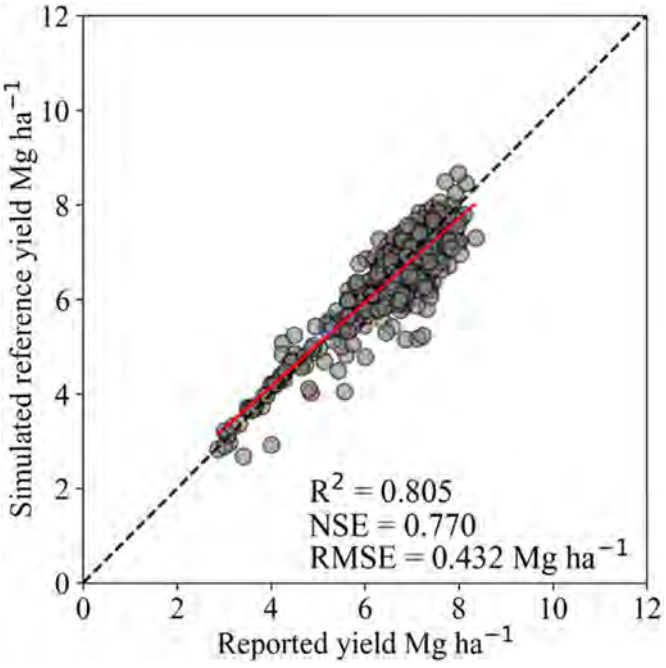

Fig. 4. Rice yield comparison. Comparison between simulated rice yields using the calibrated RSCM and reported rice yields for 106 counties and provinces (gray dots) in South Korea (96 counties) and North Korea (10 provinces) from 2011 to 2016. The black dotted line is a one-to-one line, and the red line represents the trend line.

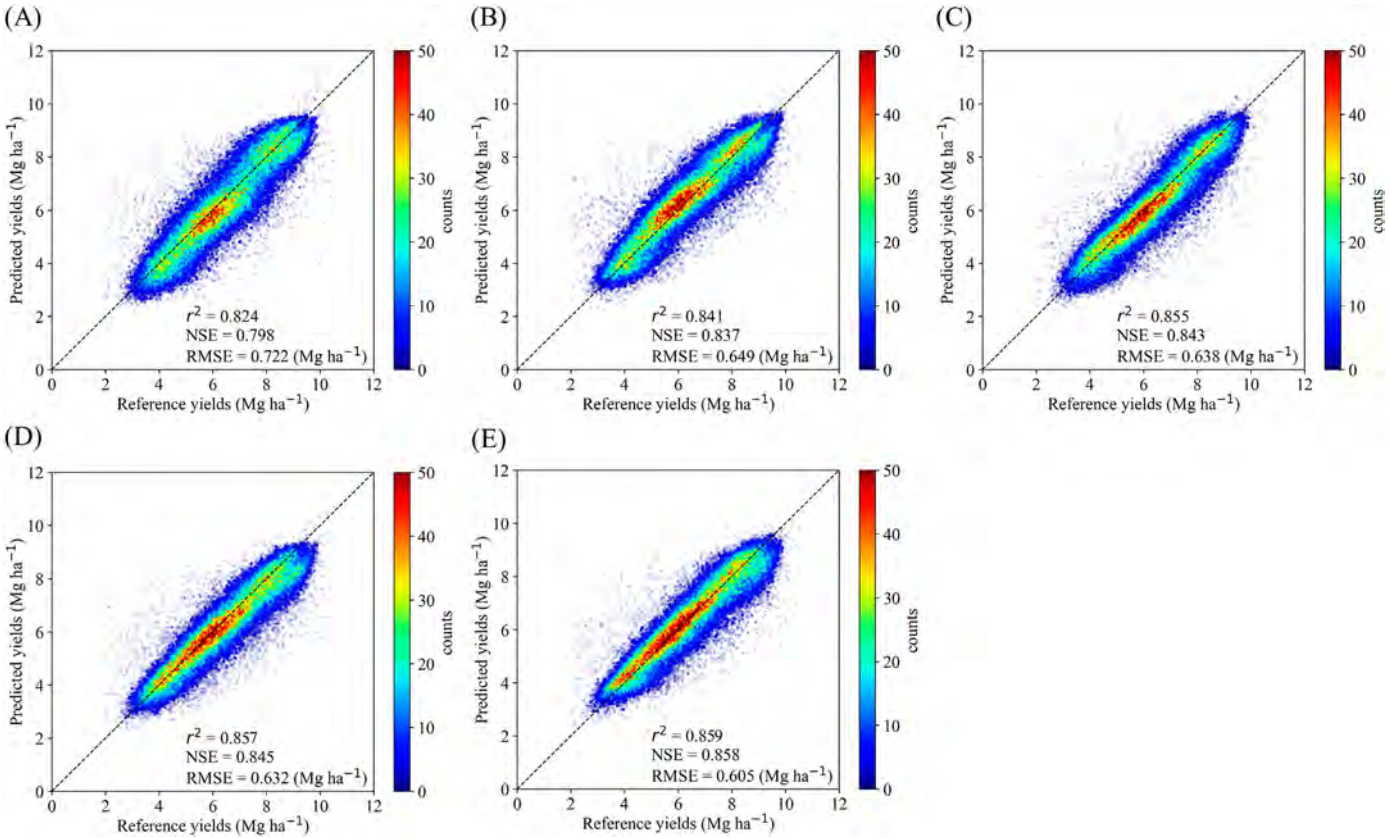

Fig. 5. Density plots for comparisons of early predicted rice yields at the pixel scale using the calibrated RSCM and five DL models with reference rice yields for the Korean Peninsula in 2017 (n = 57,726). (A) FFNN model. (B) 1D-CNN model. (C) LSTM model. (D) 1D-CNN + LSTM model. (E) LSTM+1D-CNN model.

(Chu and Yu, 2020; Wang et al., 2020). In contrast, the FFNN model showed the lowest performance, with R^2 = 0.859, NSE = 0.858, and RMSE = 0.605 Mg ha^{-1} (Fig. 5A). Therefore, LSTM+1D-CNN was selected to predict the rice yield at the pixel scale. For reference, the determined optimal hyperparameters used in the LSTM+1D-CNN model are summarized in Table S1 of the supplementary file.

There are some limitations of the DL model used in this study. First it learns the output of the crop model, so the performance of the DL model cannot exceed the performance of the crop model. Therefore, in order to improve the DL model, the crop model's performance is the most important factor. Second, although the optimal values and results were presented considering the learning time, selected DL structures and hyperparameters may be expected to be suboptimal, indicating that room for performance improvement remains to be achieved through more diverse structures and hyperparameter tuning. As feasible approaches to further improve the predictive performance, employing a multi-model ensemble or transfer learning models would present powerful prediction performance, although we have not covered such techniques in the current study (Yin et al., 2017; Wang et al., 2018). Recently, auto-ML techniques for determining the optimal structure as well as hyperparameters by themselves have been continuously developed (He et al., 2021). Because more advanced algorithms are rapidly being developed, better research results are expected to be reported quickly.

3.3. Prediction of rice yield using DL model

Fig. 6 shows the maps of the early prediction study results of rice yields at the pixel and county scales for the whole study area. In these maps, a clear pattern is observed, i.e., the rice yields in South Korea are higher than those in North Korea for both spatial scales. The pixel-scale rice yield map was specifically estimated at a spatial resolution of 500 m, which is the same scale as that of the reference yields of the RSCM with increasing or decreasing patterns within each administrative unit (Fig. 6A). In contrast, the result of rice yield prediction at the county scale showed only the representative values of each administrative district (Fig. 6B). Thus, the existing prediction model at the county scale is limited in terms of interpreting the spatial variation in the rice yield; the county-scale yields not only lacked the significant advantage of satellite images but also were less sensitive to spatial variations in the rice yields within each county region.

Furthermore, histograms for pixel-scale yields (gray bars) and county-scale yields (red vertical bars) were extracted for each of the highest rice production regions, namely Pyongyang province in North Korea (red polygon region in Fig. 6A and C) and Gimje county in South Korea (blue polygon region in Fig. 6B and D). In Fig. 6A and C, the histogram for North Korea is widely distributed in the shape of the bell, whereas the one for South Korea has two narrow peaks. In the case of North Korea, the overall geographic variation in rice production is large, indicating regional variations in the agricultural infrastructure and management systems within provinces. In the case of South Korea, two different types of varieties are mainly cultivated, namely early maturing (around 11%) and medium-late (around 89%) varieties; the former tends to have a somewhat lower yield than the latter (Nam et al., 2019). Therefore, the two peaks in the histogram can be mainly interpreted as owing to the difference in the varieties. Furthermore, as can be seen from the histograms and red bars in Fig. 6C and D, a single value for the yield of an administrative district may not be suitable to represent the variation within the regions. We believe that the pixel-scale crop yield would provide spatially quantified information within regions.

Fig. S2 in the supplementary file shows that the predictive performance at the county scale (B) was better than that at the pixel scale (A). This is because predicting the average representative value of the administrative units is easier than predicting the pixel-scale rice yield

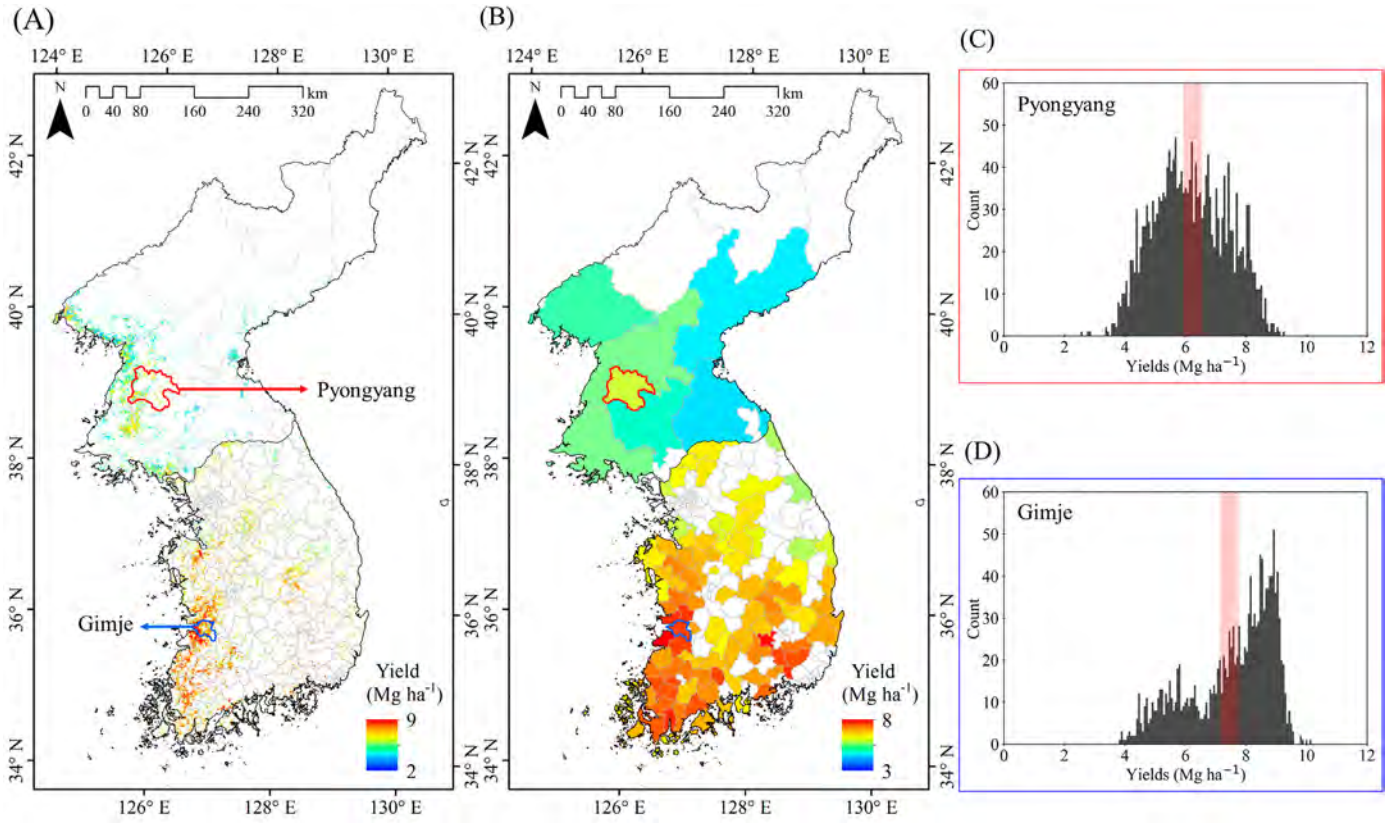

Fig. 6. Rice yield maps for early prediction by combining the RSCM and DL model incorporating satellite images for South and North Korea in 2017. (A) Pixel-scale rice yield maps. (B) County-scale rice yield maps. (C), (D) Histograms of the pixel- (gray bars) and county- (red bars) scale yields over the blue and red polygons of (A) and (B) for the highest rice-yielding regions in South and North Korea, respectively.

with more diverse and uncertain values within a county. However, county-scale crop yields cannot represent variations within region, especially in regions where various varieties are cultivated. Therefore, our approach can potentially achieve accurate and precise spatial crop yield prediction.

3.4. Analysis of relative input importance and yields for South and North Korea

We analyzed the RI of the input variables according to the different agricultural environments in South and North Korea using Eq. (7), as shown in Fig. 7. In North Korea, there was a noticeable variation in the importance of each variable, i.e., LSWI, T_{max}, and TPDs exerted a significant influence on the rice yield compared to that in South Korea, whereas the five VIs (NDVI, OSAVI, RDVI, MTVI, and EVI), geographic coordinates, and T_{min} were of higher importance in South Korea than in North Korea.

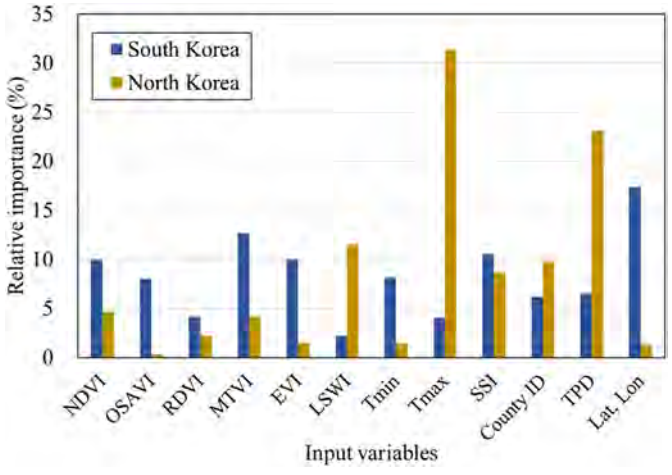

Fig. 7. Relative importance (RI) of input variables for South and North Korea. The relative importance of the input variables when a specific variable was removed from the inputs of the DL model for rice yield prediction in South and North Korea in 2017.

The VIs appear more important than the LSWI related to water for South Korea, implying that the water supply is not an essential factor in determining the rice yield because the irrigation facilities are well equipped and the precipitation is sufficient; hence, the importance of the VIs is relatively high. North Korea appears to have poor irrigation facilities in general (Ryu et al., 2019) and the precipitation is relatively low as well (UN FAO, 2017). Therefore, the effect of LSWI on the rice yield is higher in North Korea than in South Korea. With regard to temperature, many studies have reported that the plant stress from T_{min} at night has a more adverse effect on the rice yield than that from T_{max} during the day (Wolanin et al., 2020; Wu et al., 2016; Xu et al., 2020). In South Korea, T_{min} was a more important factor than T_{max}, as reported previously. However, in North Korea, T_{max} appeared to be important for predicting rice yields. According to the Korea Rural Economic Institute (KREI, https://www.krei.re.kr) in 2017, transplanting was difficult in North Korea owing to abnormally high temperatures from the winter of 2016 to June 2017. Thus, we interpreted this as T_{max} being the most important variable in the prediction of the rice yield. The TPD also showed high RI with regard to rice yield prediction, as the abnormally high temperatures in North Korea in 2017 may have prevented timely transplantation. The geographic coordinates showed the highest RI in South Korea. As many rice varieties are cultivated in the regions of South Korea, we believe that these variables reflect regional characteristics. Meanwhile, as the rice varieties cultivated in North Korea are not as diverse as those in South Korea, based on an example of the yield distribution histogram (Fig. 6C and D), the RI of the geographic coordinates seems to be low.

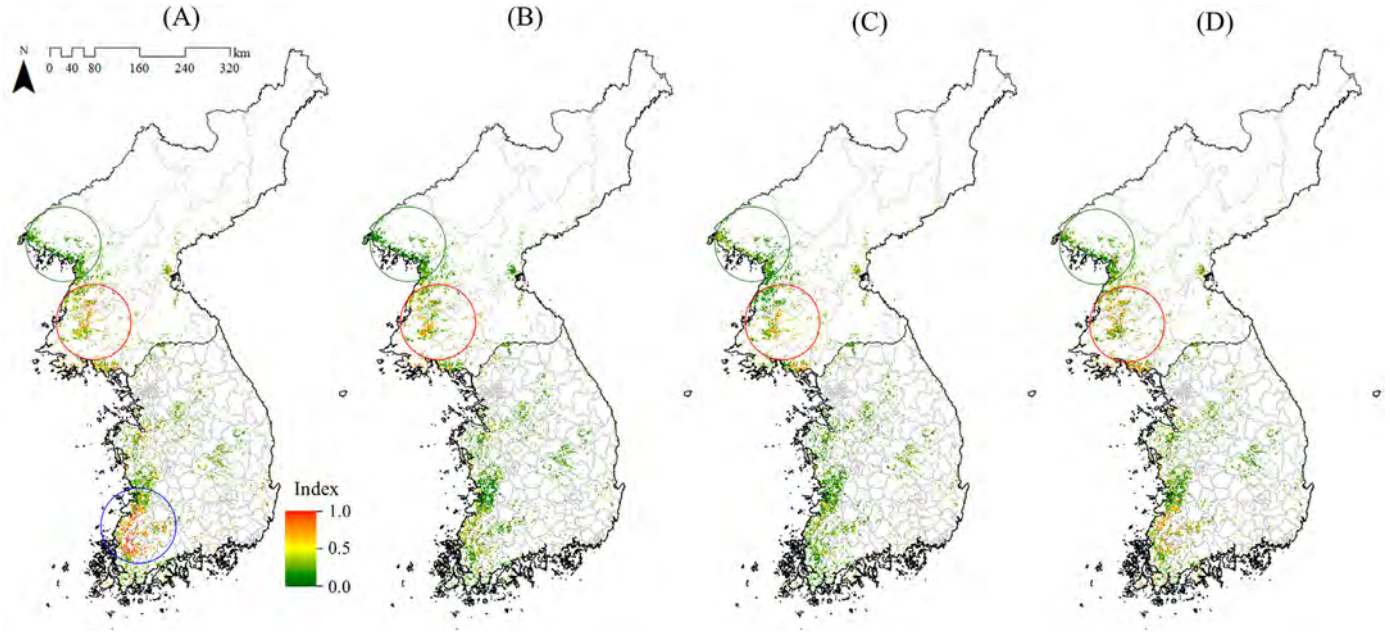

Fig. 8. Geographical error variations. Error variations in removed (A) vegetation indices, (B) land surface water index, (C) maximum temperature, and (D) transplanting date of the DL model for predicting pixel-scale rice yields with satellite images for South and North Korea in 2017.

Distinctive spatial patterns of the input RI are well represented for the VIs, LSWI, T_{max}, and TPD (Fig. 7). Fig. 8 shows the index maps of the error variation for the four main differences in the RI. Similar to the results of Fig. 7, LSWI, T_{max}, and TPD are shown as red index areas, indicating that these are important variables that explain the rice yield of North Korea (red circles in Fig. 8). By contrast, the VIs of South Korea, denoted by the blue circles in Fig. 8A, have higher index values, implying that the VIs affect the rice yield owing to the well-developed irrigation facilities in South Korea. The green circles (Pyongan province) in Fig. 8 indicate that in North Korea, the variation errors of the selected LSWI, T_{max}, and TPD are low, similar to those in South Korea. Here, the rice cultivation area is spatially clustered; it is not only a large-scale rice production area but also a high production area in North Korea. In other words, despite the poor agricultural facilities in North Korea overall, we can infer that there are adequate irrigation facilities in large-scale rice cultivation areas. High-resolution satellite imagery of the area shows that irrigation facilities are well constructed in the green circles (see Fig. S3 in the supplementary file).

Finally, when the yield prediction performance of the DL model was analyzed by dividing it between South and North Korea, the performance of the model for North Korea was better than that for South Korea (Fig. S4A and S4B); this is because South Korea is well equipped in terms of field management, through human interventions such as the use of fertilizers and pesticides. It also indicates that the importance of environment variables is relatively low in simulating a DL model in the case of South Korea due to the better management of agricultural infrastructures. On the other hand, it is interpreted that North Korea responds sensitively to the influence of environmental variables such as weather, and the yield prediction performance of the model is relatively high. Such a trend was more evident when comparing the yields at the county scale (Fig. S4C and S4D). In the comparison of the reported yields at the county scale and predicted yields averaged by pixels within counties, the yields in South Korea were clustered at the center, which could mean that the quantity is being managed. The developed agricultural management systems reduce the variability due to high-yields in all the region. Meanwhile, in North Korea, it was spread out with distinct linearity. Therefore, in future studies, we expect that the performance of the model can be further improved if the variable of human intervention according to the agricultural environment can be additionally modeled for regions with well-established infrastructures for crop systems.

4. Conclusion

Thus far, rice yield prediction based on DL models with satellite images has been conducted at the county scale. However, accurate diagnosis of crop yields remains challenging, as the variation and uncertainty within regions are unknown, especially for inaccessible regions such as North Korea. To overcome this limitation, this study has proposed a novel approach for predicting rice yield at pixel scale by combining a crop model and a DL model, incorporating satellite images of South and North Korea showing their different agricultural environments. We trained a process-based crop model integrated with satellite images using the DL technique and proved that early prediction of the pixel-scale crop yield (which is difficult using existing crop models) is possible through combination with the DL model. In particular, the process-based crop model was able to predict the crop yield even in inaccessible regions such as North Korea, where data acquisition is nearly impossible. In addition, analysis of the RI showed that the input variables determining crop yields differ between South and North Korea due to the difference in agricultural environment. Finally, in the future, the suggested methodology including the early prediction of crop yields and the analysis method for the RI could be transferrable to various regions and crops by applying other crop models or advanced DL models.

CRediT authorship contribution statement

Seungtaek Jeong: Methodology, Investigation, Validation, Visualization, Writing – review & editing. **Jonghan Ko:** Formal analysis, Writing – review & editing. **Jong-Min Yeom:** Conceptualization, Methodology, Investigation, Supervision, Writing – original draft, Writing – review & editing, Funding acquisition.

Declaration of competing interest

The authors declare that there is no conflict of interest.

Acknowledgments

We are grateful to the editors and anonymous referees for their helpful comments and suggestions. This work was supported by a grant from the Korea Aerospace Research Institute (FR21J00). The basic

science research program through the National Research Foundation of Korea (NRF-2021R1A2C2004459) financially supported Jonghan's study.

Appendix A. Supplementary data

Supplementary data to this article can be found online at https://doi.org/10.1016/j.scitotenv.2021.149726.

References

Arigbe, O.D., Oyeneyin, M.B., Arana, I., Ghazi, M.D., 2019. Real-time relative permeability prediction using deep learning. J. Petrol. Explor. Prod. Technol. 9 (2), 1271–1284.

Bolton, D.K., Friedl, M.A., 2013. Forecasting crop yield using remotely sensed vegetation indices and crop phenology metrics. Agric. Forest Meteorol. 173, 74–84.

Bose, P., Kasabov, N.K., Bruzzone, L., Hartono, R.N., 2016. Spiking neural networks for crop yield estimation based on spatiotemporal analysis of image time series. IEEE Trans. Geosci. Remote Sensing 54 (11), 6563–6573.

Cai, Y., Guan, K., Lobell, D., Potgieter, A.B., Wang, S., Peng, J., Xu, T., Asseng, S., Zhang, Y., You, L., Peng, B., 2019. Integrating satellite and climate data to predict wheat yield in Australia using machine learning approaches. Agric. Forest Meteorol. 274, 144–159.

Cao, J., Zhang, Z., Tao, F., Zhang, L., Luo, Y., Zhang, J., Han, J., Xie, J., 2021. Integrating multi-source data for rice yield prediction across China using machine learning and deep learning approaches. Agric. Forest Meteorol. 297, 108275. http://www.ncbi.nlm.nih.gov/pubmed/108275.

Chandrasekar, K., Sesha Sai, M.V.R., Roy, P.S., Dwevedi, R.S., Surface Water, L., 2010. Land surface water index (LSWI) response to rainfall and NDVI using the MODIS vegetation index product. Int. J. Remote Sens. 31 (15), 3987–4005.

Chu, Z., Yu, J., 2020. An end-to-end model for rice yield prediction using deep learning fusion. Comput. Electron. Agric. 174. http://www.ncbi.nlm.nih.gov/pubmed/105471.

Doraiswamy, P.C., Hatfield, J.L., Jackson, T.J., Akhmedov, B., Prueger, J., Stern, A., 2004. Crop condition and yield simulations using Landsat and MODIS. Remote Sens. Environ. 92 (4), 548–559.

Doraiswamy, P.C., Sinclair, T.R., Hollinger, S., Akhmedov, B., Stern, A., Prueger, J., 2005. Application of MODIS derived parameters for regional crop yield assessment. Remote Sens. Environ. 97 (2), 192–202.

Elbern, H., Schmidt, H., Talagrand, O., Ebel, A., 2000. 4D-variational data assimilation with an adjoint air quality model for emission analysis. Environ. Model. Softw. 15 (6–7), 539–548.

Fageria, N.K., 2007. Green manuring in crop production. J. Plant Nutr. 30 (5), 691–719.

Ferencz, C., Bognár, P., Lichtenberger, J., Hamar, D., Timár, G., Molnár, G., Pásztor, S.Z., Steinbach, P., Székely, B., Ferencz, O.E., Ferencz-Árkos, I., Tarcsai, G.Y., 2004. Crop yield estimation by satellite remote sensing. Int. J. Remote Sens. 25 (20), 4113–4149.

Filippi, P., Jones, E.J., Wimalathunge, N.S., Somarathna, P.D.S.N., Pozza, L.E., Ugbaje, S.U., Jephcott, T.G., Paterson, S.E., Whelan, B.M., Bishop, T.F.A., 2019. An approach to forecast grain crop yield using multi-layered, multi-farm data sets and machine learning. Precis. Agric. 20 (5), 1015–1029.

Franch, B., Vermote, E.F., Becker-Reshef, I., Claverie, M., Huang, J., Zhang, J., Justice, C., Sobrino, J.A., 2015. Improving the timeliness of winter wheat production forecast in the United States of America, Ukraine and China using MODIS data and NCAR growing degree day information. Remote Sens. Environ. 161, 131–148.

Gao, B.C., 1996. NDWI—a normalized difference water index for remote sensing of vegetation liquid water from space. Remote Sens. Environ. 58 (3), 257–266.

Gao, Y., Wang, S., Guan, K., Wolanin, A., You, L., Ju, W., Zhang, Y., 2020. The ability of sun-induced chlorophyll fluorescence from OCO-2 and MODIS-EVI to monitor spatial variations of soybean and maize yields in the midwestern USA. Remote Sens. 12 (7), 1111.

Guan, K., Wu, J., Kimball, J.S., Anderson, M.C., Frolking, S., Li, B., Hain, C.R., Lobell, D.B., 2017. The shared and unique values of optical, fluorescence, thermal and microwave satellite data for estimating large-scale crop yields. Remote Sens. Environ. 199, 333–349.

Haboudane, D., Miller, J.R., Pattey, E., Zarco-Tejada, P.J., Strachan, I.B., 2004. Hyperspectral vegetation indices and novel algorithms for predicting green LAI of crop canopies: modeling and validation in the context of precision agriculture. Remote Sens. Environ. 90 (3), 337–352.

He, X., Zhao, K., Chu, X., 2021. AutoML: a survey of the state-of-the-art. Knowl. Based Syst. 212, 106622.

Huang, J., Wang, H., Dai, Q., Han, D., 2014. Analysis of NDVI data for crop identification and yield estimation. IEEE J. Sel. Top. Appl. Earth Obs. Remote Sens. 7 (11), 4374–4384.

Huang, J., Gómez-Dans, J.L., Huang, H., Ma, H., Wu, Q., Lewis, P.E., Liang, S., Chen, Z., Xue, J.H., Wu, Y., Zhao, F., Xie, X., 2019. Assimilation of remote sensing into crop growth models: current status and perspectives. Agric. Forest Meteorol. 276–277, 107609.

Huete, A., Didan, K., Miura, T., Rodriguez, E.P., Gao, X., Ferreira, L.G., 2002. Overview of the radiometric and biophysical performance of the MODIS vegetation indices. Remote Sens. Environ. 83 (1–2), 195–213.

Ioffe, S., Szegedy, C., 2015. Batch normalization: accelerating deep network training by reducing internal covariate shift. arXiv Preprint ArXiv:1502.03167.

Jeong, S., Kang, S., Jang, K., Lee, H., Hong, S., Ko, D., 2012. Development of variable threshold models for detection of irrigated paddy rice fields and irrigation timing in heterogeneous land cover. Agric. Water Manag. 115, 83–91.

Jeong, J.H., Resop, J.P., Mueller, N.D., Fleisher, D.H., Yun, K., Butler, E.E., Timlin, D.J., Shim, K.M., Gerber, J.S., Reddy, V.R., Kim, S.H., 2016. Random forests for global and regional crop yield predictions. PLoS ONE 11 (6), e0156571.

Jeong, S., Ko, J., Yeom, J.M., 2018. Nationwide projection of rice yield using a crop model integrated with geostationary satellite imagery: a case study in South Korea. Remote Sens. 10 (10), 1665.

Jeong, S., Ko, J., Kang, M., Yeom, J., Ng, C.T., Lee, S.H., Lee, Y.G., Kim, H.Y., 2020. Geographical variations in gross primary production and evapotranspiration of paddy rice in the Korean Peninsula. Sci. Total Environ. 714, 136632.

Jiang, D., Yang, X., Clinton, N., Wang, N., 2004. An artificial neural network model for estimating crop yields using remotely sensed information. Int. J. Remote Sens. 25 (9), 1723–1732.

Jiang, H., Hu, H., Zhong, R., Xu, J., Xu, J., Huang, J., Wang, S., Ying, Y., Lin, T., 2020. A deep learning approach to conflating heterogeneous geospatial data for corn yield estimation: a case study of the US Corn Belt at the county level. Glob. Change Biol. 26 (3), 1754–1766.

Khaki, S., Wang, L., 2019. Crop yield prediction using deep neural networks. Front. Plant Sci. 10, 621.

Khaki, S., Wang, L., Archontoulis, S.V., 2020. A cnn-rnn framework for crop yield prediction. Front. Plant Sci. 10, 1750. https://doi.org/10.3389/fpls.2019.01750.

Kim, H., Ko, J., Jeong, S., Yeom, J., Ban, J., Kim, H., 2015. Simulation and mapping of rice growth and yield based on remote sensing. J. Appl. Remote. Sens. 9 (1), 096067. http://www.ncbi.nlm.nih.gov/pubmed/096067.

Kim, M., Ko, J., Jeong, S., Yeom, J., Kim, H., 2017. Monitoring canopy growth and grain yield of paddy rice in South Korea by using the GRAMI model and high spatial resolution imagery. GISci. Remote Sens. 54 (4), 534–551.

Kim, N., Ha, K., Park, N., Cho, J., Hong, S., Lee, Y., 2019. A comparison between major artificial intelligence models for crop yield prediction: case study of the midwestern United States, 2006–2015. ISPRS Int. J. Geo Inf. 8 (5), 240.

Kim, N., Na, S., Park, C., Huh, M., Oh, J., Ha, K., Cho, J., Lee, Y., 2020. An artificial intelligence approach to prediction of corn yields under extreme weather conditions using satellite and meteorological data. Appl. Sci. 10 (11), 3785.

Kogan, F., Salazar, L., Roytman, L., 2012. Forecasting crop production using satellite-based vegetation health indices in Kansas, USA. Int. J. Remote Sens. 33 (9), 2798–2814.

Kumar, P., Prasad, R., Choudhary, A., Gupta, D.K., Mishra, V.N., Vishwakarma, A.K., Singh, A.K., Srivastava, P.K., 2019. Comprehensive evaluation of soil moisture retrieval models under different crop cover types using C-band synthetic aperture radar data. Geocarto Int. 34 (9), 1022–1041.

Lichtenthaler, H.K., 1996. Vegetation stress: an introduction to the stress concept in plants. J. Plant Physiol. 148 (1–2), 4–14.

Lobell, D.B., Asner, G.P., 2003. Climate and management contributions to recent trends in U.S. agricultural yields. Science 299 (5609), 1032.

Lobell, D.B., Roberts, M.J., Schlenker, W., Braun, N., Little, B.B., Rejesus, R.M., Hammer, G.L., 2014. Greater sensitivity to drought accompanies maize yield increase in the U.S Midwest. Science 344 (6183), 516–519.

Lobell, D.B., Thau, D., Seifert, C., Engle, E., Little, B., 2015. A scalable satellite-based crop yield mapper. Remote Sens. Environ. 164, 324–333.

Maas, S.J., 1992. GRAMI: A Crop Growth Model That Can Use Remotely Sensed Information. ARSUS Department of Agriculture Agricultural Research Service, USA.

Maas, S.J., 1993. Within-season calibration of modeled wheat growth using remote sensing and field sampling. Agron. J. 85 (3), 669–672.

Maimaitijiang, M., Sagan, V., Sidike, P., Hartling, S., Esposito, F., Fritschi, F.B., 2020. Soybean yield prediction from UAV using multimodal data fusion and deep learning. Remote Sens. Environ. 237, 111599. http://www.ncbi.nlm.nih.gov/pubmed/111599.

Nam, J.K., Park, H.S., Baek, M.K., Cho, Y.C., Kim, W.J., Kim, J.J., Kim, B.K., Kim, K.Y., Shin, W.C., Ko, J.C., Lee, G.M., Park, S.G., Lee, C.M., Kim, C.S., Suh, J.P., Lee, J.H., 2019. Bacterial blight-resistant medium maturing rice cultivar 'Haepum' with high grain quality. Korean J. Breed. Sci. 51 (3), 222–233.

Nash, J.E., Sutcliffe, J.V., 1970. River flow forecasting through conceptual models part I – a discussion of principles. J. Hydrol. 10 (3), 282–290.

Nelson, A., Gumma, M.K., 2015. A Map of Lowland Rice Extent in the Major Rice Growing Countries of Asia. 37. IRRI, Los Baños, Philippines.

Nevavuori, P., Narra, N., Lipping, T., 2019. 163, 104859. http://www.ncbi.nlm.nih.gov/pubmed/104859.

Nguyen, V.C., Jeong, S., Ko, J., Ng, C.T., Yeom, J., 2019. Mathematical integration of remotely sensed information into a crop modelling process for mapping crop productivity. Remote Sens. 11 (18), 2131.

Peel, M.C., Finlayson, B.L., McMahon, T.A., 2007. Updated world map of the Köppen-Geiger climate classification. Hydrol. Earth Syst. Sci. 11 (5), 1633–1644.

Peng, D., Huang, J., Li, C., Liu, L., Huang, W., Wang, F., Yang, X., 2014. Modelling paddy rice yield using MODIS data. Agric. Forest Meteorol. 184, 107–116.

Quintero, E., Thessen, A.E., Arias-Caballero, P., Ayala-Orozco, B., 2014. A statistical assessment of population trends for data deficient mexican amphibians. PeerJ 2, e703.

Ren, J., Chen, Z., Zhou, Q., Tang, H., 2008. Regional yield estimation for winter wheat with MODIS-NDVI data in Shandong, China. Int. J. Appl. Earth Obs. Geoinf. 10 (4), 403–413.

Rondeaux, G., Steven, M., Baret, F., 1996. Optimization of soil-adjusted vegetation indices. Remote Sens. Environ. 55 (2), 95–107.

Roujean, J.L., Breon, F.M., 1995. Estimating PAR absorbed by vegetation from bidirectional reflectance measurements. Remote Sens. Environ. 51 (3), 375–384.

Rouse Jr., J.W., 1974. Monitoring the vernal advancement and retrogradation (green wave effect) of natural vegetation. NASA/GSFC Type III Final Report, Greenbelt, Md, p. 371.

Ryu, J.H., Han, K.S., Lee, Y.W., Park, N.W., Hong, S., Chung, C.Y., Cho, J., 2019. Different agricultural responses to extreme drought events in neighboring counties of south and North Korea. Remote Sens. 11 (15), 1773.

Sakamoto, T., Nguyen, N.V., Kotera, A., Ohno, H., Ishitsuka, N., Yokozawa, M., 2007. Detecting temporal changes in the extent of annual flooding within the Cambodia and the

Vietnamese Mekong Delta from MODIS time-series imagery. Remote Sens. Environ. 109 (3), 295–313.
Sammut, C., Webb, G.I., 2011. Encyclopedia of Machine Learning. Springer Science Business Media, New York.
Schwalbert, R.A., Amado, T., Corassa, G., Pott, L.P., Prasad, P.V.V., Ciampitti, I.A., 2020. Satellite-based soybean yield forecast: integrating machine learning and weather data for improving crop yield prediction in southern Brazil. Agric. Forest Meteorol. 284, 107886. http://www.ncbi.nlm.nih.gov/pubmed/107886.
Song, X., Zhang, G., Liu, F., Li, D., Zhao, Y., Yang, J., 2016. Modeling spatio-temporal distribution of soil moisture by deep learning-based cellular automata model. J. Arid Land 8 (5), 734–748.
Su, Y.X., Xu, H., Yan, L.J., 2017. Support vector machine-based open crop model (SBOCM): case of rice production in China. Saudi J. Biol. Sci. 24 (3), 537–547.
Sun, J., Di, L., Sun, Z., Shen, Y., Lai, Z., 2019. County-level soybean yield prediction using deep CNN-LSTM model. Sensors 19 (20), 4363.
UN Food and Agriculture Organization (FAO), 2017. Global information and early warning system (GIEWS). Spec, Alert, p. 340.
Vincenzi, S., Zucchetta, M., Franzoi, P., Pellizzato, M., Pranovi, F., De Leo, G.A., Torricelli, P., 2011. Application of a random forest algorithm to predict spatial distribution of the potential yield of ruditapes philippinarum in the Venice lagoon. Italy. Ecol. Modell. 222 (8), 1471–1478.
Wang, A.X., Tran, C., Desai, N., Lobell, D., Ermon, S., 2018. Deep transfer learning for crop yield prediction with remote sensing data. Proc. 1st ACM SIGCAS Conf. Comput. Sust. Soc., pp. 1–5.
Wang, X., Huang, J., Feng, Q., Yin, D., 2020. Winter wheat yield prediction at county level and uncertainty analysis in main wheat-producing regions of China with deep learning approaches. Remote Sens. 12 (11), 1744.
Wheeler, J.A., Salter, P.J., 1974. Effects of shortening the maturity period on harvesting costs of autumn cauliflowers. Sci. Hortic. 2 (1), 83–92.
Wolanin, A., Mateo-García, G., Camps-Valls, G., Gómez-Chova, L., Meroni, M., Duveiller, G., Liangzhi, Y., Guanter, L., 2020. Estimating and understanding crop yields with explainable deep learning in the Indian Wheat Belt. Environ. Res. Lett. 15 (2), 024019. http://www.ncbi.nlm.nih.gov/pubmed/024019.
Wu, C., Cui, K., Wang, W., Li, Q., Fahad, S., Hu, Q., Huang, J., Nie, L., Peng, S., 2016. Heat-induced phytohormone changes are associated with disrupted early reproductive development and reduced yield in rice. Sci. Rep. 6 (1), 34978.
Xiao, X., Boles, S., Liu, J., Zhuang, D., Frolking, S., Li, C., Salas, W., Moore III, B., 2005. Mapping paddy rice agriculture in southern China using multi-temporal MODIS images. Remote Sens. Environ. 95 (4), 480–492.
Xiao, X., Hagen, S., Zhang, Q., Keller, M., Moore III, B., 2006. Detecting leaf phenology of seasonally moist tropical forests in South America with multi-temporal MODIS images. Remote Sens. Environ. 103 (4), 465–473.
Xin, F., Xiao, X., Dong, J., Zhang, G., Zhang, Y., Wu, X., Li, X., Zou, Z., Ma, J., Du, G., Doughty, R.B., Zhao, B., Li, B., 2020. Large increases of paddy rice area, gross primary production, and grain production in Northeast China during 2000–2017. Sci. Total Environ. 711, 135183.
Xu, J., Henry, A., Sreenivasulu, N., 2020. Rice yield formation under high day and night temperatures – a prerequisite to ensure future food security. Plant Cell Environ. 43 (7), 1595–1608.
Yang, Q., Shi, L., Han, J., Zha, Y., Zhu, P., 2019. Deep convolutional neural networks for rice grain yield estimation at the ripening stage using UAV-based remotely sensed images. Field Crops Res. 235, 142–153.
Yeom, J.M., Seo, Y.K., Kim, D.S., Han, K.S., 2016. Solar radiation received by slopes using COMS imagery, a physically based radiation model, and GLOBE. J. Sens. 2016, 1–15.
Yeom, J.M., Jeong, S., Jeong, G., Ng, C.T., Deo, R.C., Ko, J., 2018. Monitoring paddy productivity in North Korea employing geostationary satellite images integrated with GRAMI-rice model. Sci. Rep. 8 (1), 16121.
Yeom, J.M., Jeong, S., Deo, R.C., Ko, J., 2021. Mapping rice area and yield in northeastern Asia by incorporating a crop model with dense vegetation index profiles from a geostationary satellite. GISci. Remote Sens. 58 (1), 1–27.
Yin, Z., Zhao, M., Wang, Y., Yang, J., Zhang, J., 2017. Recognition of emotions using multimodal physiological signals and an ensemble deep learning model. Comput. Methods Prog. Biomed. 140, 93–110.
Zhang, X., Zhang, Q., 2016. Monitoring interannual variation in global crop yield using long-term AVHRR and MODIS observations. ISPRS J. Photogramm. 114, 191–205.
Zhang, Q., Li, J., Liu, J.S., Du, X., Zhao, L., Wang, N., Dong, T., 2017. Crop classification and acreage estimation in North Korea using phenology features. GISci. Remote Sens. 54, 381–406.
Zhang, C., Zhu, C., Xu, X., Liu, Y., Xiao, J., Tillo, T., 2018. Visual aesthetic understanding: sample-specific aesthetic classification and deep activation map visualization. Signal Process. Image Commun. 67, 12–21.
Zhao, Y., Chen, S., Shen, S., 2013. Assimilating remote sensing information with crop model using ensemble Kalman filter for improving LAI monitoring and yield estimation. Ecol. Model. 270, 30–42.